Research Square

Preprints are preliminary reports that have not undergone peer review.
They should not be considered conclusive, used to inform clinical practice,
or referenced by the media as validated information.

Strong-Field Amplitude Modulation of Massless Klein--Gordon Waves near a Schwarzschild Horizon

Benliang Li
University of South China
Jun Liu
ljj3321250650163.com

University of South China
HengJian SiTu
University of South China

Research Article

Keywords:

Posted Date: August 25th, 2026

DOI: https://doi.org/10.21203/rs.3.rs-10315000/v1

License: This work is licensed under a Creative Commons Attribution 4.0 International License.
Read Full License

Additional Declarations: No competing interests reported.

Strong-Field Amplitude Modulation of Massless Klein–Gordon Waves near a Schwarzschild Horizon

Ben-liang Li, HengJian SiTu, Jun Liu
School of Mathematics and Physics, University of South China, Hengyang 421001, China
Corresponding author: Jun Liu, lj332125065@163.com

Abstract

We study massless Klein–Gordon waves outside a Schwarzschild black hole. The aim is to understand how a wave mode can depart from the null-geodesic, or ray-optics, description when its wavelength is not negligible compared with the gravitational length scale. The work is motivated by gravitational length stretching (GLS), in which the amplitude factor of a curved-spacetime mode is interpreted as a geometry-induced modulation of the spatial probability profile. We use Cartesian Schwarzschild coordinates and select a beam-like solution sector. The stationary mode is written with a complex wave number, $k(z) = a(z) + ib(z)$. The real part $a(z)$ controls the phase, while $b(z)$ controls the amplitude factor $B(z) = \exp\big[-\int b(z')dz'\big]$. We solve the resulting amplitude–phase equations numerically in the exterior region. Far from the horizon, and in the short-wavelength regime, the solution agrees with the standard null-geodesic result. For low-frequency modes, the phase gradient differs strongly from the eikonal wave number, and the amplitude develops clear spatial modulation. The group velocity is computed from a small family of nearby frequency solutions, $a(z;\omega)$, through $v_g = (\partial a/\partial\omega)^{-1}$. The near-horizon growth of this Schwarzschild-coordinate group velocity is interpreted as a sign that the eikonal approximation has broken down, not as a violation of local causality. These results indicate that the GLS amplitude mechanism has a strong-field analogue for massless scalar waves.

1 Introduction

Quantum fields in curved spacetime provide the standard framework for studying matter waves on a classical gravitational background. In this framework the spacetime metric is not quantized, but the field modes propagate according to generally covariant wave equations. This setting underlies many central results in black-hole and early-universe physics, including Hawking radiation, the Unruh effect, and particle creation in curved backgrounds [1–6]. The massless Klein–Gordon (KG) field is the simplest example. It is also a useful model because it separates the effect of spacetime geometry on wave propagation from complications due to spin, gauge constraints, or self-interaction.

In the short-wavelength limit, a massless field recovers the classical ray picture. If a scalar field is written in WKB form as $\Phi = A\exp(iS/\epsilon)$, the leading order in ϵ gives

$$g^{\mu\nu}\partial_\mu S\partial_\nu S = 0, \tag{1}$$

and the wave vector $k_\mu = \partial_\mu S$ is tangent to null geodesics. The next order gives a transport equation for the amplitude. Thus the null geodesic is the leading phase trajectory of the wave, not the whole

wave solution [7–9]. When the wavelength becomes comparable to the length scale over which the metric changes, the separation between phase propagation and amplitude transport can fail. Then diffraction, backscattering, and curvature-induced amplitude changes become part of the physical behavior of the mode.

This issue is familiar in black-hole wave physics. Scalar, electromagnetic, spinor, and gravitational perturbations outside a Schwarzschild black hole can be reduced to radial wave equations with effective curvature potentials. These equations explain scattering, absorption, greybody factors, and quasinormal behavior [10–15]. At high frequency, many features of the scattering problem are well described by null geodesics and semiclassical approximations. At low frequency, however, the field nature of the mode is essential; for example, greybody factors and absorption cross sections depend on the wave equation rather than only on classical ray capture [16, 17]. The present work belongs to this second regime. It asks how the local phase and amplitude of a beam-like KG mode behave when the eikonal approximation is no longer reliable.

The phase of quantum matter in a gravitational field has a long history in interferometry and relativistic quantum mechanics. A common expression is the covariant phase integral $\phi = \hbar^{-1} \int p_\mu dx^\mu$, which connects quantum phases with classical action and proper-time effects [18–20]. Recent high-precision atom and neutron experiments have made gravitational phase effects increasingly relevant at laboratory scales [21–24]. Yet the amplitude of a curved-spacetime mode is also important. It is fixed by current conservation and by the spatial measure used to normalize states. The amplitude can therefore carry geometric information that is not captured by the phase alone.

This paper is motivated by gravitational length stretching (GLS) [25]. In that work, the WKB mode contains an amplitude factor $B_k(t, \mathbf{x})$ satisfying the covariant continuity equation $\nabla_\mu(B_k^2 k^\mu) = 0$. When states are normalized with the proper spatial measure, B_k^2 acts as a curvature-induced modulation of the spatial probability profile. The published analysis focused mainly on weak-field massive-particle systems, especially ultracold neutrons in Earth's gravitational field. Here we ask whether the same amplitude mechanism has a strong-field analogue for massless KG waves outside a Schwarzschild horizon.

We use Cartesian Schwarzschild coordinates and select a beam-like solution sector aligned with the radial z direction. The transverse-uniformity condition is imposed as a constraint on the mode family, not as a consequence of the full KG equation. Within that selected sector, the field depends only on t and the propagation coordinate z, and the transverse derivatives vanish. This produces a reduced exterior equation that still contains the metric-gradient terms generated by the Schwarzschild geometry. The reduction is designed to compare directly with a classical radial null ray while retaining the amplitude transport of the wave.

The stationary mode is written with a complex local wave number,

$$k(z) = a(z) + ib(z). \tag{2}$$

The real part $a(z)$ gives the phase gradient, and the imaginary part $b(z)$ determines the amplitude factor $B(z) = \exp\big[-\int b(z')dz'\big]$. Substitution into the reduced KG equation gives coupled nonlinear equations for a and b, or equivalently a single second-order equation for a. The group velocity shown below is computed by solving this equation for several nearby frequencies and evaluating $v_g(z) = (\partial a(z;\omega)/\partial\omega)^{-1}$ by finite differences on the same radial grid.

The term "non-geodesic" is used in this paper in a wave-mechanical sense. It means that the massless KG mode departs from the single-ray geometric-optics approximation. It does not mean that a classical massless point particle violates the null-geodesic equation. The velocity compared

with the classical result is a Schwarzschild-coordinate group velocity, not a locally measured speed. Local causality remains controlled by the light cone of the metric.

The paper is organized as follows. Section 2 gives the Schwarzschild metric in Cartesian coordinates and derives the beam-sector radial equation. Section 3 derives the equations for $a(z)$ and $b(z)$. Section 4 explains the conserved-current and GLS probability interpretation. Section 5 describes the numerical method and the group-velocity calculation. Section 6 presents the numerical results. Section 7 discusses the relation to GLS, black-hole scattering, coordinate interpretation, and future extensions.

2 Schwarzschild metric and beam-sector radial reduction

The Schwarzschild line element may be written in spherical coordinates (t, r, θ, ϕ) as

$$ds^2 = -\left(1 - \frac{r_s}{r}\right) c^2 dt^2 + \left(1 - \frac{r_s}{r}\right)^{-1} dr^2 + r^2 d\Omega^2, \tag{3}$$

where $r_s = 2GM/c^2$. In matrix form, with $x^0 = ct$ suppressed in the notation used below, the corresponding metric components are

$$g_{\mu\nu} = \begin{pmatrix} (r_s - r)/r & 0 & 0 & 0 \\ 0 & r/(r - r_s) & 0 & 0 \\ 0 & 0 & r^2 & 0 \\ 0 & 0 & 0 & r^2 \sin^2\theta \end{pmatrix}. \tag{4}$$

To compare the wave solution with the classical geodesic picture, it is useful to work in Cartesian-like coordinates rather than only in spherical coordinates. In spherical coordinates, the natural elementary solution is a spherical wave. Its flux is distributed over a sphere whose area grows as $4\pi r^2$, so its intensity decreases as $1/r^2$. This describes radiation emitted in all directions, like light from an isotropic point source. Such a wave is not the closest wave analogue of a classical particle or light ray following a single geodesic path, because its probability or energy density spreads over the angular directions during propagation.

By contrast, a highly collimated beam is closer to the classical geodesic limit. A laser beam, for example, is prepared so that most of its intensity remains concentrated around one propagation direction over long distances. In the idealized limit, this resembles a plane-wave or beam-like mode whose transverse profile changes much more slowly than its longitudinal phase. Such a mode does not represent radiation spreading isotropically from a point source. It represents a wave packet selected around a preferred path. This is the wave configuration most suitable for comparison with the motion of a classical object or photon along a geodesic.

For this reason, we formulate the Klein–Gordon equation in Cartesian Schwarzschild coordinates and select a beam-like sector propagating along the z-axis. The z-axis plays the role of the reference geodesic path, while the transverse x- and y-directions describe the beam cross-section. This coordinate choice allows us to impose a transverse-uniformity condition and to study how the longitudinal phase and amplitude evolve along the propagation direction. Physically, the setup may be compared with a well-collimated electromagnetic or scalar-wave beam sent from the Earth's surface toward a distant satellite, as illustrated in Fig. 1. Although a real beam has finite transverse width and diffraction, the idealized Cartesian beam sector captures the one-dimensional propagation needed to compare quantum wave behavior with the classical geodesic picture.

In Cartesian coordinates we have $x = r\sin\theta\cos\phi$, $y = r\sin\theta\sin\phi$, and $z = r\cos\theta$. The contravariant metric components are [25, 26]

$$g^{\mu\nu} = \begin{pmatrix} -\dfrac{r}{r-r_s} & 0 & 0 & 0 \\ 0 & 1-\dfrac{x^2 r_s}{r^3} & -\dfrac{xyr_s}{r^3} & -\dfrac{xzr_s}{r^3} \\ 0 & -\dfrac{xyr_s}{r^3} & 1-\dfrac{y^2 r_s}{r^3} & -\dfrac{yzr_s}{r^3} \\ 0 & -\dfrac{xzr_s}{r^3} & -\dfrac{yzr_s}{r^3} & 1-\dfrac{z^2 r_s}{r^3} \end{pmatrix}, \tag{5}$$

with $r = (x^2+y^2+z^2)^{1/2}$. The corresponding covariant components are

$$g_{\mu\nu} = \begin{pmatrix} -\dfrac{r-r_s}{r} & 0 & 0 & 0 \\ 0 & 1+\dfrac{x^2 r_s}{r^2(r-r_s)} & \dfrac{xyr_s}{r^2(r-r_s)} & \dfrac{xzr_s}{r^2(r-r_s)} \\ 0 & \dfrac{xyr_s}{r^2(r-r_s)} & 1+\dfrac{y^2 r_s}{r^2(r-r_s)} & \dfrac{yzr_s}{r^2(r-r_s)} \\ 0 & \dfrac{xzr_s}{r^2(r-r_s)} & \dfrac{yzr_s}{r^2(r-r_s)} & 1+\dfrac{z^2 r_s}{r^2(r-r_s)} \end{pmatrix}, \tag{6}$$

for which $g = \det(g_{\mu\nu}) = -1$ in the Cartesian chart.

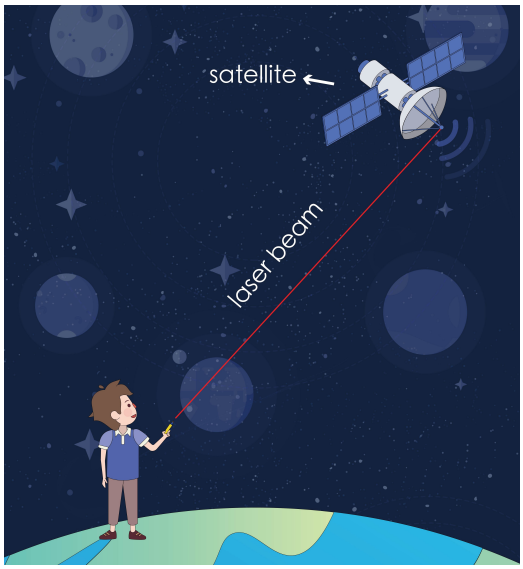


Figure 1: A narrow laser-like beam can be represented by a wave whose centroid propagates along one spatial direction. The present calculation selects the beam-like sector aligned with the radial z-axis and compares its eikonal limit with the classical null-geodesic result.

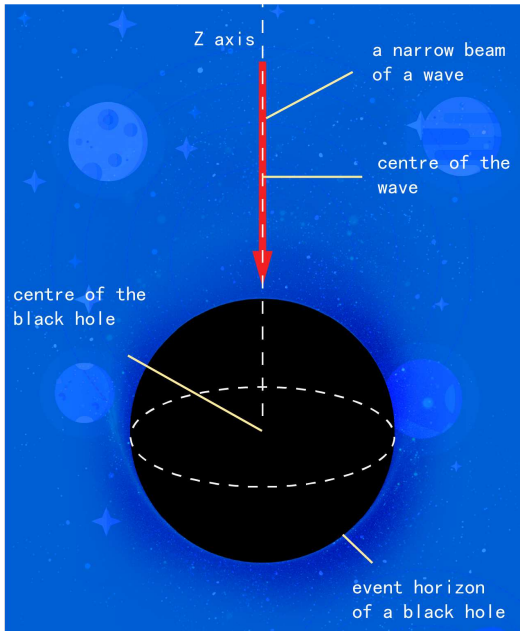


Figure 2: Radial beam geometry used in the calculation. The beam centroid is aligned with the z-axis and points toward the Schwarzschild center. The transverse-uniformity condition selects the beam-like sector used below.

The massless KG equation is

$$\Box f \equiv \frac{1}{\sqrt{-g}} \partial_\mu \left(\sqrt{-g}\, g^{\mu\nu} \partial_\nu f \right) = 0. \tag{7}$$

Since $\sqrt{-g} = 1$, this becomes

$$\partial_\mu \left(g^{\mu\nu} \partial_\nu f \right) = 0. \tag{8}$$

We now isolate the beam-like sector studied in this work. The massless KG equation in Eq. (8) governs all scalar waves in the Schwarzschild background. Its solution space is much larger than the sector considered here: it contains spherical waves, cylindrical waves, scattered waves, partial-wave modes, and wave packets with nontrivial transverse structure. Our purpose is different. We want to compare a quantum wave mode with the classical radial null-geodesic picture. For that comparison, the relevant modes are those that remain concentrated around a chosen propagation direction and have no appreciable variation across the transverse section of the beam.

To select such modes, we impose the transverse-uniformity condition

$$f(t, x, y, z) = f(t, 0, 0, z) \quad \text{for all } (x, y) \text{ within the beam cross-section.} \tag{9}$$

This is not derived from Eq. (8). It is an additional condition that restricts the full solution space to a special beam-like family. The logic is as follows.

1. Equation (8) describes the full scalar-field dynamics in the Schwarzschild geometry. Without any additional restriction, it allows many different wave configurations, including spherical, cylindrical, scattered, and transverse-profile-dependent modes.

2. We are interested in modes that resemble a classical radial ray. Such modes are expected to be concentrated around one propagation path and to have negligible transverse variation within the beam width.

3. We therefore impose Eq. (9) as a constraint selecting this sector. This does not mean that every solution of the KG equation has this form. It means that the present calculation studies the subset of modes that also satisfy the transverse-uniformity condition.

4. The nontrivial question is whether this restricted sector admits solutions compatible with the KG equation after the Schwarzschild metric terms are included. If it does, these solutions provide a useful wave analogue of a radially directed classical trajectory.

5. The following derivation constructs the reduced equation obtained from the full KG operator under this constraint, and the numerical solutions solve the resulting equations. In this sense, the existence of nontrivial beam-like modes is tested within the selected sector rather than assumed at the level of the final solution.

Once Eq. (9) is imposed, all transverse derivatives of the selected field vanish identically,

$$\partial_x f = \partial_y f = 0, \qquad \partial_x^2 f = \partial_y^2 f = \partial_x \partial_y f = 0. \tag{10}$$

These relations are exact consequences of the imposed transverse-uniformity constraint. They are not obtained by dropping small transverse derivative terms. The curvature of the background is still present, however, because the metric coefficients depend on the Schwarzschild radius $r =$

$(x^2+y^2+z^2)^{1/2}$. Thus the reduced equation retains metric-gradient contributions even though the field itself has no transverse variation in the selected beam sector. In particular, derivatives of the metric coefficients contribute when the full operator $\partial_\mu(g^{\mu\nu}\partial_\nu f)$ is evaluated on the beam axis.

Evaluating Eq. (8) on the positive z-axis, where $x = y = 0$ and $r = z$, gives

$$\left(\frac{\partial g^{zx}}{\partial x} + \frac{\partial g^{zy}}{\partial y} + \frac{\partial g^{zz}}{\partial z}\right)\partial_z f + g^{tt}\frac{1}{c^2}\partial_t^2 f + g^{zz}\partial_z^2 f = 0. \tag{11}$$

The derivative term is nonzero even on the axis because the metric varies in the transverse directions. From Eq. (5),

$$\partial_x g^{zx}|_{x=y=0} = -\frac{r_s}{z^2}, \qquad \partial_y g^{zy}|_{x=y=0} = -\frac{r_s}{z^2}, \qquad \partial_z g^{zz}|_{x=y=0} = \frac{r_s}{z^2}, \tag{12}$$

so that their sum is $-r_s/z^2$. The reduced equation is therefore

$$-\frac{z}{z-r_s}\frac{1}{c^2}\frac{\partial^2 f}{\partial t^2} - \frac{r_s}{z^2}\frac{\partial f}{\partial z} + \frac{z-r_s}{z}\frac{\partial^2 f}{\partial z^2} = 0. \tag{13}$$

This is the effective one-dimensional exterior equation used below.

3 Amplitude–phase decomposition

We seek stationary exterior modes of Eq. (13) in the form

$$f(t,z) = \exp\left[-i\left(\omega t - \int^z k(z')\,dz'\right)\right], \tag{14}$$

where ω is the Killing frequency measured at infinity and $k(z)$ may be complex. Substitution into Eq. (13) gives the Riccati-type equation

$$\frac{dk}{dz} - \frac{r_s}{z(z-r_s)}k + i\left[k^2 - \frac{\omega^2 z^2}{c^2(z-r_s)^2}\right] = 0. \tag{15}$$

This Riccati equation is equivalent to the original second-order mode equation wherever the logarithmic derivative is defined. Its advantage is that it separates the phase change from the amplitude change.

The leading eikonal solution is obtained by dropping the derivative and transport terms compared with the local dispersion term. This gives

$$k_c(z) = \frac{z\omega}{c(z-r_s)}. \tag{16}$$

The corresponding phase is

$$f_c(t,z) = \exp\left\{-i\omega\left[t - \frac{z}{c} - \frac{r_s}{c}\ln(z-r_s)\right]\right\}, \tag{17}$$

and the associated Schwarzschild-coordinate velocity is

$$v_{gp} \equiv \frac{\partial\omega}{\partial k_c} = c\left(1 - \frac{r_s}{z}\right). \tag{18}$$

This is the standard radial coordinate speed of an outgoing or ingoing null ray in Schwarzschild coordinates, up to the sign convention for the propagation direction.

Writing

$$k(z) = a(z) + ib(z), \tag{19}$$

with real a and b, Eq. (15) separates into

$$a' - \frac{r_s}{z(z-r_s)}a - 2ab = 0, \tag{20}$$

$$b' - \frac{r_s}{z(z-r_s)}b + a^2 - b^2 - \frac{\omega^2 z^2}{c^2(z-r_s)^2} = 0. \tag{21}$$

The first of these gives

$$b(z) = \frac{1}{2a}\frac{da}{dz} - \frac{r_s}{2z(z-r_s)}. \tag{22}$$

Eliminating b yields a single second-order nonlinear equation for $a(z)$,

$$\frac{1}{2a}\frac{d^2a}{dz^2} - \frac{3}{4a^2}\left(\frac{da}{dz}\right)^2 + a^2 - \frac{\omega^2 z^2}{c^2(z-r_s)^2} + \frac{r_s(4z-r_s)}{4z^2(z-r_s)^2} = 0. \tag{23}$$

Equations (22) and (23) are the central equations solved below. Equation (23) is also the location at which the leading eikonal approximation can fail most clearly: if the derivative terms are small, $a \simeq k_c$; if they are comparable to the dispersion term, the full nonlinear equation is required.

The complete stationary mode can be written as

$$f_\omega(t,z) = B(z)\exp\left[-i\left(\omega t - \int^z a(z')dz'\right)\right], \tag{24}$$

where

$$B(z) = \exp\left[-\int^z b(z')dz'\right]. \tag{25}$$

The function $a(z)$ controls the local oscillatory phase, while $B(z)$ controls the amplitude. The two functions are not independent. Equation (20) shows that a change in $a(z)$ also changes the amplitude gradient $b(z)$.

4 Conserved current and GLS probability measure

For a complex scalar field, the KG equation admits the conserved current

$$J^\mu = \frac{i}{2}\left(f^*\nabla^\mu f - f\nabla^\mu f^*\right), \qquad \nabla_\mu J^\mu = 0. \tag{26}$$

For a positive-frequency wave packet with a slowly varying envelope, this current has the local form $J^\mu \sim B^2 k^\mu$. This is the same structural origin as the GLS continuity equation $\nabla_\mu(B_k^2 k^\mu) = 0$ in the WKB formulation [25]. In the present strong-field calculation, B^2 is interpreted through the proper probability measure on a chosen spatial slice, rather than as a coordinate-invariant probability density by itself.

For a reduced one-dimensional packet $F(t,z) = \int D(\omega) f_\omega(t,z) d\omega$, the probability in an interval is normalized as

$$P_t(z_1, z_2) = \frac{\int_{z_1}^{z_2} |F(t,z)|^2 \sqrt{\gamma}\, dz}{\int |F(t,z)|^2 \sqrt{\gamma}\, dz}, \tag{27}$$

where $\sqrt{\gamma}\, dz$ is the proper spatial measure along the reduced direction. For a narrow-band packet centered on ω_0, the amplitude factor gives the leading modulation,

$$P_t(z_1, z_2) \propto \int_{z_1}^{z_2} B^2(z) \sqrt{\gamma}\, dz, \tag{28}$$

up to the usual interference effects associated with the finite bandwidth. Thus, by "probability modulation" we mean modulation of the properly normalized spatial probability profile, not the coordinate function $B^2(z)$ alone.

This point matters near a black-hole horizon. Schwarzschild time slices and static observers become singular at $z = r_s$, so coordinate profiles are not automatically local observables. The calculation is therefore an exterior Schwarzschild-coordinate test of GLS-like amplitude transport. A horizon-regular coordinate system is needed for a fully invariant statement at the horizon.

5 Numerical method

Equation (23) is integrated from the far exterior toward the horizon. The calculation shown in the figures uses $r_s = 1\,\mathrm{m}$ and a central frequency $\omega_0 = 10^5\,\mathrm{s}^{-1}$; in this notation ω is an angular frequency. A useful dimensionless parameter is

$$\Omega \equiv \frac{\omega r_s}{c}. \tag{29}$$

For the plotted central frequency and $r_s = 1\,\mathrm{m}$, $\Omega \simeq 3.3 \times 10^{-4}$. The displayed example is therefore a deliberately low-frequency case, far from the eikonal limit. In the opposite regime $\Omega \gg 1$, one expects the derivative terms in Eq. (23) to become relatively less important and the eikonal relation $a \simeq k_c$ to be restored over a larger exterior region.

The integration begins at $z_0/r_s = 100$ and proceeds inward to $z/r_s > 1$. Far from the source, the mode is required to match the eikonal solution,

$$a(z_0) = k_c(z_0), \qquad a'(z_0) = k_c'(z_0), \tag{30}$$

with k_c given by Eq. (16). These two conditions specify the second-order problem. The equation is solved with a fourth-order Runge–Kutta method with adaptive step-size control. The function $b(z)$ is then reconstructed from Eq. (22). Numerical consistency is checked by substituting the reconstructed pair (a, b) back into Eqs. (20) and (21). A further consistency check is to substitute the reconstructed full mode Eq. (24) into the original reduced wave equation Eq. (13) and monitor the residual.

The group velocity shown below is evaluated from a finite family of nearby frequency solutions. Specifically, the equation is solved for

$$\omega_j = \omega_0 + j\Delta\omega, \qquad j = -N, \ldots, N, \tag{31}$$

with the same outer boundary prescription and with all solutions interpolated onto the same radial grid. The derivative is then evaluated as

$$v_g(z;\omega_0) = \left(\frac{\partial a(z;\omega)}{\partial \omega}\right)^{-1}\Bigg|_{\omega_0} \simeq \frac{\omega_+ - \omega_-}{a(z;\omega_+) - a(z;\omega_-)}, \tag{32}$$

with additional neighboring frequencies used to test stability of the derivative. In the calculations used to generate the displayed curve, the derivative was stable under changes of the frequency spacing within the numerical resolution of the plot. Thus the group-velocity curve is not inferred from a single fixed-frequency solution. It represents the local dispersion slope of the numerically obtained family $a(z;\omega)$.

All results refer to the exterior Schwarzschild region. Because Schwarzschild coordinates are singular at $z = r_s$, the near-horizon behavior of coordinate quantities such as v_g is not a locally measured superluminal velocity. A formulation in Eddington–Finkelstein, Painleve–Gullstrand, or Kruskal coordinates is needed to discuss horizon crossing in an invariant way [9, 27].

6 Numerical results

6.1 Phase-gradient component

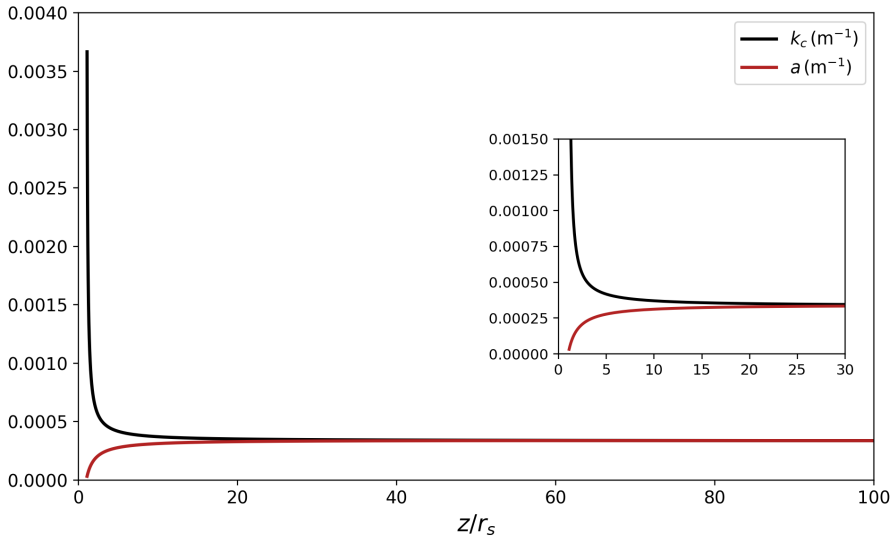


Figure 3: Comparison between the eikonal wave number $k_c(z)$ and the numerically obtained real phase-gradient component $a(z)$ for $r_s = 1\,\mathrm{m}$ and $\omega = 10^5\,\mathrm{s}^{-1}$. The two curves agree in the far exterior. The low-frequency solution departs from the eikonal prediction as the mode approaches the strong-field region.

Figure 3 compares the eikonal wave number $k_c(z)$ with the real part $a(z)$ obtained from the full reduced amplitude–phase equation. In the far exterior, the two agree, as required by the

correspondence with geometric optics. Closer to the horizon, the eikonal prediction increases rapidly because $k_c \propto z/(z - r_s)$. For a fixed Killing frequency, this corresponds to the familiar divergence of the locally measured frequency by static observers near the horizon; it is different from the redshift of radiation emitted with fixed local frequency and received at infinity.

The numerical low-frequency phase gradient bends away from the eikonal curve. This behavior indicates that the mode can no longer be described by the leading-order null-ray approximation. The important point is not that a point particle changes its geodesic law. Rather, the scalar wave enters a regime where phase change and amplitude transport are strongly coupled. In the language of Eq. (23), the derivative terms and the algebraic dispersion term become comparable, so the usual local relation between ω and k no longer gives an adequate description.

6.2 Amplitude-transport component and probability modulation

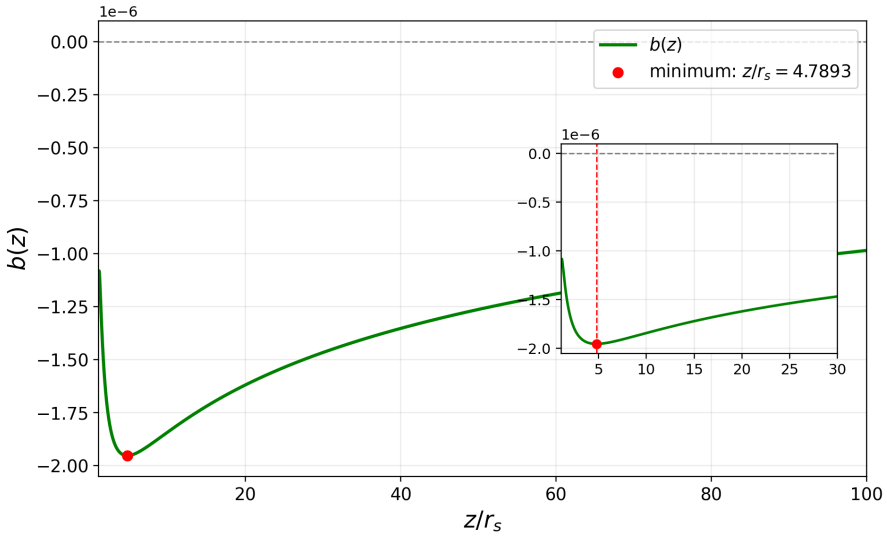


Figure 4: Imaginary component $b(z)$ of the complex wave number reconstructed from Eq. (22). This component controls the amplitude modulation $B(z) = \exp\left[-\int b dz\right]$.

Figure 4 shows the imaginary component $b(z)$. Far from the black hole, $b(z)$ tends to zero and the mode approaches an ordinary plane wave. Closer to the horizon, $b(z)$ becomes nonzero, showing that curvature produces an amplitude-transport term. Through Eq. (25), this component controls the spatial modulation of $B^2(z)$.

Figure 5 displays the squared amplitude factor. The curve increases with z/r_s, meaning that B^2 is suppressed as the mode approaches the horizon. This fixes an important point of interpretation: in the GLS convention, smaller B^2 in a stronger gravitational region corresponds to stretching of the proper probability profile, not compression. Thus the figure is consistent with the weak-field GLS interpretation in Ref. [25]: curvature redistributes the probability density through the amplitude factor and the proper spatial measure.

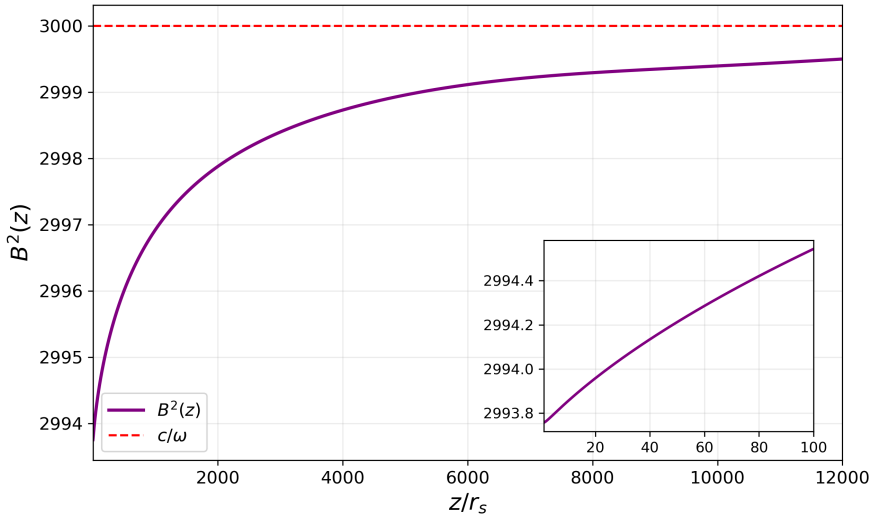


Figure 5: Squared amplitude factor $B^2(z)$ as a function of z/r_s. With the normalization used in the numerical plot, B^2 increases with distance from the horizon and is suppressed in the stronger-field region. This is the convention consistent with GLS: smaller local B^2 corresponds to a stretched proper probability profile when combined with the proper spatial measure.

The result is therefore described as curvature-induced amplitude modulation. The reduced curved-space wave equation strongly couples the phase-gradient part $a(z)$ to the amplitude part $b(z)$, providing a strong-field analogue of the amplitude modulation underlying GLS.

6.3 Group velocity from nearby frequencies

The group velocity of the reduced wave packet is defined by

$$v_g(z) = \left(\frac{\partial a(z;\omega)}{\partial \omega} \right)^{-1} . \tag{33}$$

As described in Sec. 5, this derivative is computed from several nearby numerical solutions, not from one curve. Figure 6 compares the resulting v_g with the eikonal/null-geodesic coordinate velocity $v_{gp} = c(1 - r_s/z)$.

In the far exterior, the two velocities agree, confirming that the reduced KG mode reproduces the usual null-geodesic result in the geometric-optics regime. Near the horizon, the red curve tends to zero in Schwarzschild coordinates, whereas the numerical group-velocity diagnostic grows. This growth does not mean local superluminal propagation or faster-than-light information transfer. It reflects the fact that, in this low-frequency strong-field regime, the mapping between frequency and local phase gradient is no longer the eikonal mapping $a \simeq k_c$. The single-ray description breaks down, and a full wave treatment is required.

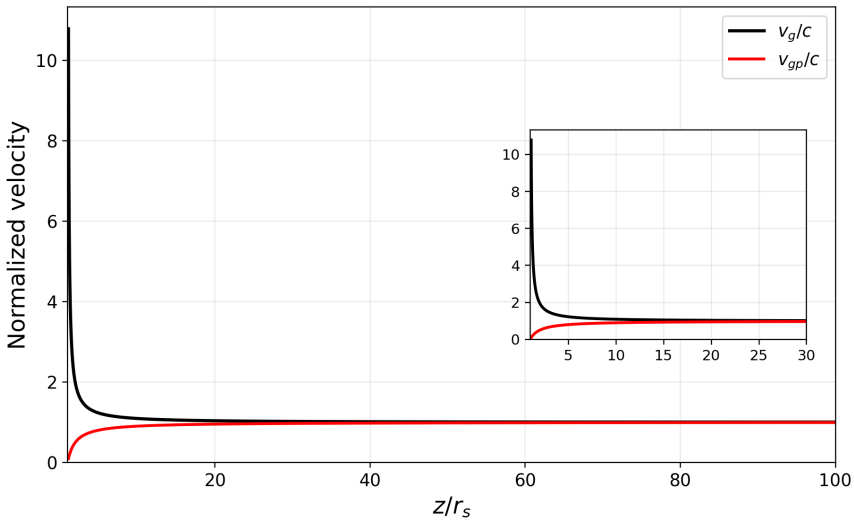


Figure 6: Normalized coordinate velocities as functions of z/r_s. The red curve shows the classical Schwarzschild-coordinate null velocity $v_{gp}/c = 1 - r_s/z$. The black curve shows the group velocity v_g/c computed from the finite-frequency-family derivative $v_g = (\partial a/\partial\omega)^{-1}$. The growth of v_g near the horizon is interpreted as a coordinate diagnostic of eikonal breakdown.

7 Discussion

7.1 Relation to gravitational length stretching

The GLS framework interprets the curved-spacetime amplitude factor B_k as a physical modulation of quantum probability density when states are normalized with the proper spatial measure [25]. The present calculation uses that framework as its starting point and moves to a different regime: a massless field, a strong Schwarzschild background, and a non-WKB numerical treatment. The result is not a repetition of the weak-field derivation. It tests whether the amplitude part of the mode remains dynamically important when the field is close to a horizon and the wavelength is large compared with the gravitational scale.

The numerical results support this extension. The squared amplitude factor $B^2(z)$ is not constant. It is suppressed in the stronger-field region near $z = r_s$, while the phase-gradient part $a(z)$ departs from the eikonal wave number $k_c(z)$. In the GLS convention, a smaller local value of B^2 corresponds to a broader properly normalized spatial probability profile. The strong-field result therefore has the same qualitative meaning as the weak-field GLS effect, but it appears here through the full coupled phase-amplitude equations rather than through a leading WKB transport equation.

The phase-amplitude system does not introduce a separate conservation law in which momentum is literally converted into probability amplitude. The equations show instead that the phase-gradient sector and the amplitude-transport sector are coupled by the curved-space KG equation. In weak fields this coupling can be small and perturbative. Near the horizon, and for low-frequency modes, it becomes large enough that a single null ray no longer provides an adequate description of the wave.

7.2 Relation to black-hole scattering and greybody factors

The standard treatment of a massless scalar field in Schwarzschild spacetime expands the field in spherical harmonics and introduces the tortoise coordinate

$$r_* = r + r_s \ln\left(\frac{r}{r_s} - 1\right). \tag{34}$$

The radial mode then satisfies a Regge–Wheeler-type equation,

$$\frac{d^2\Psi_{\ell\omega}}{dr_*^2} + \left[\frac{\omega^2}{c^2} - V_\ell(r)\right]\Psi_{\ell\omega} = 0, \tag{35}$$

where, for a minimally coupled scalar field,

$$V_\ell(r) = \left(1 - \frac{r_s}{r}\right)\left[\frac{\ell(\ell+1)}{r^2} + \frac{r_s}{r^3}\right] \tag{36}$$

up to the convention used for r_s and c. This formulation is well suited for computing scattering cross sections, absorption probabilities, quasinormal modes, and greybody factors [10–16].

The beam-sector method used here has a different purpose. It does not replace the partial-wave treatment. Instead, it follows the local logarithmic derivative of an on-axis beam-like mode and separates it into phase and amplitude pieces. This makes the comparison with the radial null-geodesic coordinate velocity direct. It also makes visible the amplitude modulation that would be hidden if one looked only at the real WKB phase. In this sense, the present calculation is complementary to the standard scattering approach: scattering theory describes asymptotic fluxes and mode mixing, whereas the present method describes local phase-amplitude transport along a selected radial sector.

The low-frequency regime is especially important. In black-hole scattering, low-frequency scalar waves are known to show behavior that cannot be reduced to a bundle of classical rays; absorption, reflection, and greybody filtering are wave effects. The present calculation identifies another local aspect of the same general fact: the phase gradient and amplitude gradient of the mode become strongly coupled when the eikonal approximation fails.

7.3 Coordinate setting and physical interpretation

The calculation is performed in Schwarzschild coordinates in the exterior region $z > r_s$. This coordinate choice is useful because it allows a direct comparison with the standard Schwarzschild-time radial null velocity $c(1 - r_s/z)$. It also gives a clear definition of the frequency ω as the Killing frequency measured by observers at infinity.

The group velocity plotted in this paper is therefore a coordinate group velocity. It is computed from the frequency dependence of the numerical phase gradient through $v_g = (\partial a/\partial\omega)^{-1}$. Near the horizon, Schwarzschild coordinates become singular, and the classical Schwarzschild-coordinate null velocity tends to zero. The growth of the numerical group-velocity diagnostic is interpreted in this coordinate setting. It signals that the relation $a \simeq k_c$ has failed and that the ray-optics description is no longer adequate. It is not a local superluminal velocity. In a local freely falling frame, causal propagation remains controlled by the light cone of the Schwarzschild metric.

This distinction is also relevant to Hawking radiation and greybody factors. Those phenomena are usually formulated by comparing modes near the horizon and at infinity, with the horizon behavior treated most cleanly in regular coordinates or in the tortoise coordinate [3, 5, 6, 14]. The

present work does not compute Hawking radiation. It studies classical field modes of the KG equation on a fixed exterior background. Nevertheless, the same lesson applies: close to the horizon, coordinate choices matter, and physical statements are most clearly made in terms of invariant currents, fluxes, or properly normalized wave packets.

7.4 Scope and possible extensions

The scalar field is treated as a test field on a fixed Schwarzschild background. Backreaction is not included. This is the standard first step in studying wave propagation in curved spacetime. A more complete semiclassical treatment would include the renormalized stress-energy tensor and the semiclassical Einstein equation [1–4].

Several extensions are natural. First, the same phase-amplitude decomposition can be repeated in tortoise coordinates or in ingoing Eddington–Finkelstein coordinates. That would separate effects tied to Schwarzschild slicing from effects that survive in a horizon-regular description. Second, one can scan the dimensionless parameter $\Omega = \omega r_s/c$ over a wide range. The figures presented here correspond to the low-frequency regime, $\Omega \ll 1$. A wider scan would show how the solution approaches the eikonal limit as Ω increases. Third, massive scalar fields would introduce the Compton wavelength as another scale, and spinor fields would introduce tetrads, spin connections, and spin-curvature coupling [28]. Finally, Kerr spacetime would add frame dragging, angular momentum exchange, and superradiance [11, 17, 27].

The result is also relevant to analogue-gravity and quantum-simulation settings, where effective metrics can be engineered and wave propagation can be tracked directly [29, 30]. Such systems may provide a practical way to test how amplitude transport behaves when an effective horizon or rapidly varying metric profile is present.

8 Conclusion

We have analyzed massless KG modes in the exterior Schwarzschild geometry using a complex-wave-vector decomposition. The real component $a(z)$ controls phase accumulation, while the imaginary component $b(z)$ controls amplitude transport. The resulting reduced equations show that these two sectors become strongly coupled in the low-frequency strong-field regime.

The numerical results recover the null-geodesic/eikonal prediction in the far exterior, but they depart from it near the horizon. The squared amplitude factor $B^2(z)$ is suppressed in the stronger-field region, consistent with the GLS interpretation that smaller local amplitude density corresponds to a stretched proper probability profile. The group velocity was computed from a finite family of nearby numerical solutions through $v_g = (\partial a/\partial\omega)^{-1}$, and its near-horizon growth is best interpreted as a Schwarzschild-coordinate signal of eikonal breakdown rather than a local causal velocity.

These findings support a conservative but potentially important conclusion: the weak-field GLS mechanism has a strong-field analogue in massless scalar-wave propagation, and a full wave description is essential when the wavelength becomes comparable to the curvature scale. Further work can repeat the calculation in horizon-regular coordinates, study more general beam sectors, and extend the analysis to massive and spinning fields.

References

[1] N. D. Birrell and P. C. W. Davies. *Quantum Fields in Curved Space*. Cambridge University Press, Cambridge, UK, 1984.

[2] Leonard Parker and David J. Toms. *Quantum Field Theory in Curved Spacetime: Quantized Fields and Gravity*. Cambridge University Press, Cambridge, UK, 2009.

[3] Robert M. Wald. *Quantum Field Theory in Curved Spacetime and Black Hole Thermodynamics*. University of Chicago Press, Chicago, 1994.

[4] Stefan Hollands and Robert M. Wald. Quantum fields in curved spacetime. *Physics Reports*, 574:1–35, 2015.

[5] S. W. Hawking. Particle creation by black holes. *Communications in Mathematical Physics*, 43:199–220, 1975.

[6] W. G. Unruh. Notes on black-hole evaporation. *Physical Review D*, 14(4):870–892, 1976.

[7] Charles W. Misner, Kip S. Thorne, and John Archibald Wheeler. *Gravitation*. W. H. Freeman, San Francisco, 1973.

[8] Steven Weinberg. *Gravitation and Cosmology: Principles and Applications of the General Theory of Relativity*. John Wiley & Sons, New York, 1972.

[9] Robert M. Wald. *General Relativity*. University of Chicago Press, Chicago, 1984.

[10] Tullio Regge and John A. Wheeler. Stability of a schwarzschild singularity. *Physical Review*, 108(4):1063–1069, 1957.

[11] Subrahmanyan Chandrasekhar. *The Mathematical Theory of Black Holes*. Oxford University Press, Oxford, 1983.

[12] Joel A. H. Futterman, F. A. Handler, and Richard A. Matzner. *Scattering from Black Holes*. Cambridge University Press, Cambridge, UK, 1988.

[13] N. G. Sanchez. Absorption and emission spectra of a schwarzschild black hole. *Physical Review D*, 18(4):1030–1036, 1978.

[14] Don N. Page. Particle emission rates from a black hole: Massless particles from an uncharged, nonrotating hole. *Physical Review D*, 13(2):198–206, 1976.

[15] Atsushi Higuchi. Low-frequency scalar absorption cross sections for stationary black holes. *Classical and Quantum Gravity*, 18(17):L139–L144, 2001.

[16] Luis C. B. Crispino, Sam R. Dolan, and Ednilton S. Oliveira. Scattering of massless scalar waves by reissner–nordström black holes. *Physical Review D*, 79(6):064022, 2009.

[17] Kostas Glampedakis and Nils Andersson. Scattering of scalar waves by rotating black holes. *Classical and Quantum Gravity*, 18(10):1939–1966, 2001.

[18] Leo Stodolsky. Matter and light wave interferometry in gravitational fields. *General Relativity and Gravitation*, 11(6):391–405, 1979.

[19] J. Anandan. Curvature effects in interferometry. *Physical Review D*, 30(8):1615–1624, 1984.

[20] Peter M. Alsing, James C. Evans, and Kamal K. Nandi. The phase of a quantum mechanical particle in curved spacetime. *General Relativity and Gravitation*, 33:1459–1487, 2001.

[21] C. Overstreet, P. Asenbaum, J. Curti, M. Kim, and M. A. Kasevich. Observation of a gravitational aharonov-bohm effect. *Science*, 375(6577):226–229, 2022.

[22] Tobias Bothwell, Colin J. Kennedy, Alexander Aeppli, Dhruv Kedar, John M. Robinson, Eric Oelker, Alexander Staron, and Jun Ye. Resolving the gravitational redshift across a millimetre-scale atomic sample. *Nature*, 602(7897):420–424, 2022.

[23] V. V. Nesvizhevsky, H. G. Börner, A. K. Petukhov, H. Abele, S. Baeßler, F. J. Rueß, Th. Stöferle, A. Westphal, A. M. Gagarski, G. A. Petrov, et al. Quantum states of neutrons in the earth's gravitational field. *Nature*, 415(6869):297–299, 2002.

[24] T. Jenke, P. Geltenbort, H. Lemmel, and H. Abele. Realization of a gravity-resonance-spectroscopy technique. *Nature Physics*, 7(6):468–472, 2011.

[25] Benliang Li. Gravitational length stretching: Curvature-induced modulation of quantum probability densities. *Open Physics*, 23(1):20250224, 2025.

[26] M. P. Hobson, G. P. Efstathiou, and A. N. Lasenby. *General Relativity: An Introduction for Physicists*. Cambridge University Press, Cambridge, UK, 2006.

[27] Valeri P. Frolov and Igor D. Novikov. *Black Hole Physics: Basic Concepts and New Developments*. Kluwer Academic Publishers, Dordrecht, 1998.

[28] F. Hammad, M. Simard, R. Saadati, and A. Landry. Curved-spacetime dynamics of spin-1/2 particles in superposed states from a wkb approximation of the dirac equation. *Physical Review D*, 110(6):065005, 2024.

[29] Carlos Barceló, Stefano Liberati, and Matt Visser. Analogue gravity. *Living Reviews in Relativity*, 14(1):3, 2011.

[30] Y. H. Shi, R. Q. Yang, Z. Xiang, Z. Y. Ge, H. Li, Y. Y. Wang, et al. Quantum simulation of hawking radiation and curved spacetime with a superconducting on-chip black hole. *Nature Communications*, 14(1):3263, 2023.